Integrated Holographic Encoder for Wavelength-Hopping/Time-Spreading Optical CDMA

Yue-Kai Huang, *Student Member, IEEE*, Varghese Baby, *Student Member, IEEE*, Paul R. Prucnal, *Member, IEEE*, Christoph M. Greiner, *Member, IEEE*, Dmitri Iazikov, *Member, IEEE*, and Thomas W. Mossberg, *Member, IEEE*

***Abstract*—We report on the application of an integrated holographic device to the generation of two-dimensional (time-frequency) optical codes for use in optical code-division multiplexing based on wavelength encoding/time spreading. The dual code device is based on two holographic Bragg reflectors and allows one to encode data with either one of two complementary diagonal 16-chip temporal-spectral codes.**

***Index Terms*—Distributed structures, encoder, holographic Bragg reflector (HBR), integrated photonic circuit, optical code-division multiplexing, photonic bandgap, wavelength hopping/time spreading.**

WAVELENGTH-HOPPING/time-spreading optical code-division multiple-access (OCDMA) [1]–[3] is a two-dimensional (2-D) coding approach that employs both wavelength and time dimensions [4], [5] and provides more flexible codes and greater capacity than approaches solely based on the time or wavelength domain. 2-D OCDMA codes consist of code chips that are characterized by time-wavelength bins chosen from a 2-D time-wavelength code matrix. Robust low-cost fully integrated devices are needed for 2-D OCDMA that can apply or strip temporal-spectral codes from data by providing appropriate color-dependent time-delays.

Here we report on a wavelength-hopping time-spreading OCDMA encoder based on holographic Bragg reflectors (HBRs) [6]–[9]. HBRs are computer-generated holographic refractive index structures created throughout areal regions of slab waveguides by deep ultraviolet (DUV) photolithography. HBR-based coarse and dense multiplexing [7], [8] and spectral comparison [9] were recently demonstrated.

Previously demonstrated 2-D OCDMA decoder–encoders, based on discrete components such as thin-film filters and fiber delays [4] or fiber Bragg gratings (FBGs) [10]–[15] are of nonintegrated nature, may be complex to assemble, and typically have a large footprint dictated by the minimum fiber bending diameter. FBG-based decoder operation also requires power splitters or circulators for separation of coded–decoded signals from the decoder input which increases system complexity and cost. Arrayed waveguide gratings (AWGs) have been used as decoders with chip-based [16] as well as fiber-based temporal delays [17], [18]. Due to the large inherent AWG size and the fact that typically two separate elements provide demultiplexing, color-dependent time delaying, and recombination of delayed wavelength chips even monolithic AWG-based decoders have relatively large footprints [16]. HBR-based coding provides spectral slicing and time delay in one element in a footprint potentially an order of magnitude smaller than the AWG-based approach. Furthermore, precision lithographic fabrication and a novel apodization approach [6] provide unprecedented control over the encoder spectral transfer function through amplitude and phase apodization of individual diffractive elements comprising the HBR. This allows one to spectrally shape wavelength chips to exhibit steep falloff and have flat-top passbands so that they can be placed in immediate spectral adjacency to each other, making possible efficient use of broad-band light sources.

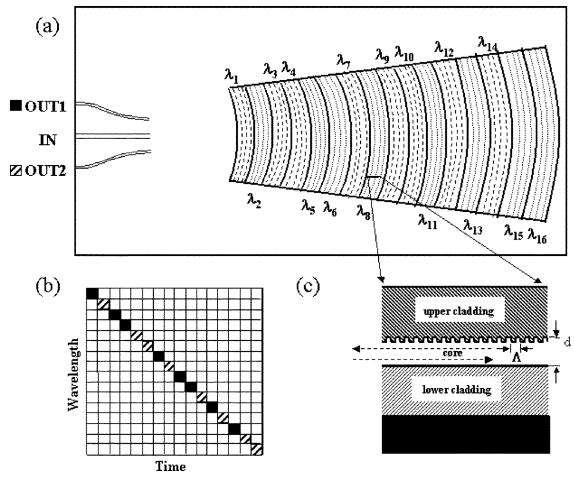

Fig. 1. Integrated holographic 2-D OCDMA encoder. (a) Top view showing input and output waveguides and HBRs; dashed (dotted) HBR segments with upper (lower) resonance wavelengths correspond to Output 1 (Output 2). (b) 2-D 16 × 16 time-wavelength code matrix. Solid (diagonally lined) segments correspond to Code 1 (Code 2). (c) Cross-sectional view; d waveguide width; Λ, grating period.

The integrated holographic OCDMA encoder is shown in a schematic top view in Fig. 1(a). Two HBRs are heavily interleaved along the input beam direction. HBR 1 (HBR2), consisting of eight interleaved grating segments indicated by dashed (dotted) lines, connects the input port (IN) to output port OUT1 (OUT2) with a port-specific transfer function corresponding to a distinct time-wavelength code. Data encoding occurs by launching a brief pulse whose spectral width equals or exceeds the code spectral width into the input port. The spectral transfer function connecting a given input–output

Manuscript received July 9, 2004; revised December 7, 2004.

Y.-K. Huang, V. Baby, and P. R. Prucnal are with the Department of Electrical Engineering, Princeton University, Princeton, NJ 08540 USA.

C. M. Greiner, D. Iazikov, and T. W. Mossberg are with LightSmyth Technologies, Inc., Eugene, OR 97041 USA (e-mail: cgreiner@lightsmyth.com).

Digital Object Identifier 10.1109/LPT.2005.843934

port pair provides color-dependent time delays for input pulse spectral components resonant with HBR grating segments. Bits coded with the first (second) code exit the device at the first (second) output port.

The 16 approximately 1.2-mm-long grating segments of the dual-HBR device each have a 1-nm 3-dB bandwidth and provide up to 16 distinct wavelength chips when programmed with different central wavelengths. At the same time, optical path length differences associated with the different grating locations provide 16 different temporal positions or time chips spaced by ~11 ps. The 16 × 16 time-wavelength matrix from which codes may be chosen in principle is shown in Fig. 1(b). In the present encoder design, two diagonal complementary time-wavelength codes were realized by decrementing the grating segment wavelength from 1532 in 1-nm steps with increasing distance from the slab region. The two resulting diagonal time-wavelength codes of Outputs 1 and 2 are shown in Fig. 1(b) as solid and diagonally lined segments. Tailored amplitude and phase apodization is imposed on the grating segments to isolate adjacent spectral chips and reduce coherent beating.

Fig. 1(c) is a partial cross-sectional view of the encoder's silica-on-silicon slab waveguide core (thickness $d = 2$ μm, 0.8% index contrast) and bilateral 15-μm-thick cladding layers. Depicted at the upper core–cladding interface are cross sections of representative lithographically scribed grating diffractive contours. The diffractive contours, with depth ~450 nm, consist of trenches etched into the core that are filled with cladding material and are spaced by $\Lambda \approx 500$nm to yield first-order grating operation of 1.5-μm signals. In Fig. 1(c), light enters from the left side and is coherently backscattered to the left by the collective action of the diffractive elements.

At the input side to the HBR slab region (diameter ~3.5 mm) the input and output channel waveguides are spaced by 30 μm and have a design width of 12.7 μm, adiabatically increased from 6 μm at the die edge via a 0.5-mm-long taper [Fig. 1(a)]. The output waveguides are slightly angled to aim at the center of the HBR section. The encoder was fabricated from a laser-written reticle employing a DUV optical stepper, standard etching, deposition, and annealing processes, and occupies a die area of only about 1.6 cm^2.

In Fig. 2(a) and (b), upper traces, we present the encoder spectral transfer functions as calculated using Fresnel–Huygens diffraction theory applied to an exact numerical model of the HBR structure as taped out for fabrication. The lower traces present the spectral transfer function of the fabricated encoder measured with a transverse magnetic (TM)-polarized tunable laser. Insertion loss shown is relative. Minimum absolute insertion loss of about 9 dB includes fiber-to-channel-waveguide coupling (about 1 dB). Transmission measurements show that remaining insertion loss arises primarily from low HBR reflectivity rather than scattering loss or absorption. High-reflectivity HBR architectures were recently demonstrated [19].

The measured device performance clearly shows the expected eight reflection bands per device output and their spectral complementarity. Deviations from design, in the form of spectral crosstalk, arise from a coupling between amplitude and phase of the fields diffracted from the grating contours induced by the chosen apodization method. Specifically, the partial writing of diffractive contours used to amplitude apodize affects the local effective waveguide index and, thus, the local Bragg resonance condition. Improved simulations [9] that fully account for the index effect show excellent agreement with the measurement indicating the high degree of fidelity at which fabrication has reproduced the encoder design. Since the effect is highly predictable it can be compensated for, e.g., by scaling the grating line separation appropriately to keep optical path distances at desired values. Encoders compensated against apodization-induced index variations will fully comply with design and, thus, exhibit significantly reduced crosstalk.

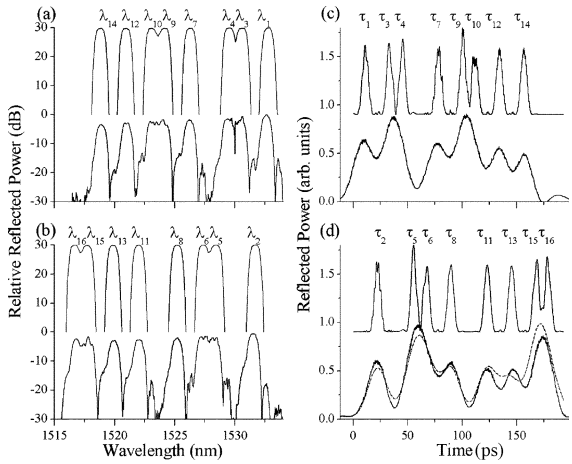

Fig. 2. Designed and measured encoder performance. (a), (b) Spectral transfer functions. (c), (d) Time-domain responses. Graphs (a) and (c): Ouput 1. Graphs (b) and (d): Output 2. All graphs: lower lines, measurement (TM polarization); upper lines, expected performance. Simulated spectral transfer functions in (a) and (b) were offset by 30 dB.

Fig. 2(c) and (d), top traces, shows the design impulse response functions for Codes 1 and 2, respectively. Total code duration is about 175 ps with a chip temporal separation of about 11 ps and chip width of about 6 ps. Measured performance (solid lines) was obtained by launching a ~500-fs-long [full-width at half-maximum (FWHM)] pulse into the encoder input and detecting the output from the encoder with a 30-GHz sampling oscilloscope. The input pulse, with spectral width of about 80 nm, was generated through fiber-based supercontinuum generation and pulse compression of an amplified mode-locked erbium-doped fiber laser.

The measurement's finite temporal resolution (measured 10/90 rise and fall time 15 and 11 ps, respectively) causes immediately adjacent time chips to appear as single peaks of higher intensity. The dashed line in Fig. 2(d) accounts for this limitation by convolving the encoder's design temporal response with a Gaussian model oscilloscope impulse response function (FWHM 15.9 ps). Agreement between data and finite-bandwidth simulation is excellent which confirms compliance of the device temporal response with the design as shown in the top trace of Fig. 2(d).

The results of Fig. 2 constitute projections of the generated codes onto the orthogonal time and wavelength axis of the 16 × 16 coding matrix. Confirmation of the expected diagonal code nature requires additional spectral analysis of the detected time chips. To simultaneously diagnose the temporal and spectral chip properties, a tunable filter is inserted between the oscilloscope and Output 2. A time and input power reference is created by splitting off a fraction of the input pulse and coupling it back onto the fiber output of the encoder before the tunable filter.

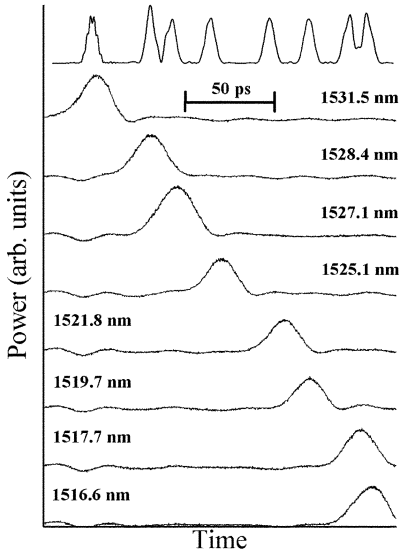

Fig. 3. Uppermost trace, design temporal response of Output 2. Lower traces, measured wavelength-filtered output from Output 2. Numerical values in the figure indicate the filter wavelength.

Fig. 3 shows the temporal response measured at Output 2 when the filter is set to the chip wavelengths shown in Fig. 2(b). The filter wavelengths (FWHM passband about 0.9 nm) were independently verified by a spectral analyzer. Chips with longer wavelengths are seen to appear earlier in time than shorter wavelength chips. Measurement and design temporal response (uppermost trace in Fig. 3) agree well, confirming the diagonal spectral–temporal code arrangement shown in Fig. 1(b).

It is important to consider coding constraints that follow specifically from HBR device properties. Let L represent the HBR length and L_{eff} the spatial coherence length of structures within the HBR. The maximum time delay provided by an HBR is $2nL/c$. Here, n is the effective waveguide index and c is the speed of light. The minimum achievable spectral chip width is the maximum of $c/2nL$ and $c/2nL_{\text{eff}}$. Recently demonstrated spatial coherence lengths of several centimeters provide minimum spectral chip widths as small as 15 pm. Nanosecond-scale code durations are provided by HBR designs based on 12-in wafers. Minimum chip duration is set approximately by $2nL_R/c$, where L_R is the grating length required to achieve desired reflectivity. Maximum code bandwidth is given approximately by $cL/2nL_R^2$. L_R depends on index contrasts and waveguide morphology, but near unity reflectivity has been observed on the length scale of a few hundred microns [19]. Timing accuracy of coded signals is limited primarily by variations in waveguide refractive index, which is typically controlled to the level of about 10^{-5}. Spectral channel control is limited at the same level by the same parameter. When codes employ durations and spectral widths large compared to these uncertainties, matching of devices for coding and decoding should be robust.

Encoder–decoder multiplicity higher than demonstrated here may be accomplished by overlaying of multiple planar holograms which enables simultaneous comparison of coded input data to many references. For encoding, the brief input pulse generates multiple differently coded outputs which can be selected by an optical switch yielding a reconfigurable $1 \times N$ encoder. Several tens of planar holograms may be overlaid on a single die of 5×20 mm providing simultaneous coding–decoding operation for an equal number of codes. Note that the color-dependent time delays provided by the present HBR device form the basis of an optical true-time delay generator as relevant for RF photonics applications such as phased-array beam steering and microwave filtering.

REFERENCES

[1] J. Shah, "Optical CDMA," *Opt. Photon. News*, vol. 14, no. 4, pp. 42–47, 2003.
[2] T. W. Mossberg and M. G. Raymer, "Optical code-division multiplexing: the intelligent optical solution," *Opt. Photon. News*, vol. 12, no. 3, pp. 50–54, 2001.
[3] A. M. Weiner and J. A. Salehi, "Optical code-division multiple access," in *Photonics in Switching*, J. E. Midwinter, Ed. San Diego, CA: Academic, 1993, vol. 2, pp. 73–118.
[4] V. Baby, C.-S. Bres, L. Xu, I. Glesk, and P. R. Prucnal, "Demonstration of differentiated service provisioning with 4-node 253 Gchip/s fast frequency-hopping time-spreading OCDMA," *Electron. Lett.*, vol. 40, no. 12, pp. 755–756, 2004.
[5] V. Baby, C.-S. Bres, I. Glesk, L. Xu, and P. R. Prucnal, "Wavelength aware receiver for enhanced 2D OCDMA system performance," *Electron. Lett.*, vol. 40, no. 6, pp. 385–387, 2004.
[6] C. Greiner, D. Iazikov, and T. W. Mossberg, "Lithographically fabricated planar holographic Bragg reflectors," *J. Lightw. Technol.*, vol. 22, no. 1, pp. 136–145, Jan. 2004.
[7] D. Iazikov, C. Greiner, and T. W. Mossberg, "Apodizable integrated filters for coarse WDM and FTTH-type applications," *J. Lightw. Technol.*, vol. 22, no. 5, pp. 1402–1407, May 2004.
[8] C. Greiner, D. Iazikov, and T. W. Mossberg, "Wavelength-division multiplexing based on apodized planar holographic Bragg reflectors," *Appl. Opt.*, vol. 43, pp. 4575–4583, 2004.
[9] T. W. Mossberg, D. Iazikov, and C. Greiner, "Planar-waveguide integrated spectral comparator," *J. Opt. Soc. Amer. A*, vol. 21, pp. 1088–1092, 2004.
[10] L. R. Chen, S. D. Benjamin, P. W. E. Smith, and J. E. Sipe, "Applications of ultrashort pulse propagation in Bragg gratings for wavelength-division-multiplexing and code-division multiple access," *IEEE J. Quantum Electron.*, vol. 34, no. 11, pp. 2117–2129, Nov. 1998.
[11] L. R. Chen, P. W. E. Smith, and C. Martijn de Sterke, "Wavelength-encoding/temporal-spreading optical code division multiple-access system with in-fiber chirped moiré gratings," *Appl. Opt.*, vol. 38, pp. 4500–4508, 1999.
[12] L. R. Chen and P. W. E. Smith, "Demonstration of incoherent wavelength-encoding/time-spreading optical CDMA using chirped Moire gratings," *IEEE Photon. Technol. Lett.*, vol. 12, no. 9, pp. 1281–1283, Sep. 2000.
[13] A. Grunnet-Jepsen, A. E. Johnson, E. S. Maniloff, T. W. Mossberg, J. J. Munroe, and J. N. Sweetser, "Demonstration of all-fiber sparse lightwave CDMA based on temporal phase encoding," *IEEE Photon. Technol. Lett.*, vol. 11, no. 10, pp. 1283–1285, Oct. 1999.
[14] A. Grunnet-Jepsen, A. E. Johnson, E. S. Maniloff, T. W. Mossberg, M. J. Munroe, and J. N. Sweetser, "Fiber Bragg grating based spectral encoder/decoder for lightwave CDMA," *Electron. Lett.*, vol. 35, pp. 1096–1097, 1999.
[15] H. Fathallah, L. A. Rusch, and S. LaRochelle, "Passive optical fast frequency-hop CDMA communications system," *J. Lightw. Technol.*, vol. 17, no. 3, pp. 397–405, Mar. 1999.
[16] K. Takiguchi, T. Shibata, and M. Itoh, "Encoder/decoder on planar lightwave circuit for time-spreading/wavelength-hopping optical CDMA," *Electron. Lett.*, vol. 38, pp. 469–470, 2002.
[17] S. Yegnanarayanan, P. D. Trinh, and B. Jalali, "Recirculating photonic filter: a wavelength-selective time delay for phased-array antennas and wavelength code-division multiple access," *Opt. Lett.*, vol. 21, pp. 740–743, 1996.
[18] S. Yegnanarayanan, A. S. Bushan, and B. Jalali, "Fast wavelength-hopping time-spreading encoding/decoding for optical CDMA," *IEEE Photon. Technol. Lett.*, vol. 12, no. 5, pp. 573–575, May 2000.
[19] C. Greiner, D. Iazikov, and T. W. Mossberg, "Low-loss silica-on-silicon two-dimensional Fabry–Perot cavity based on holographic Bragg reflectors," *Opt. Lett.*, vol. 30, no. 1, pp. 38–40, 2005.